Final Draft
of the original manuscript:

Emmler, T.; Ayala, I.; Silverman, D.; Hafner, S.; Galstyan, A.S.; Knapp, E.W.; Buntkowsky, G.:

Combined NMR and computational study for azide binding to human manganese superoxide dismutase

In: Solid State Nuclear Magnetic Resonance (2008) Elsevier

DOI: 10.1016/j.ssnmr.2008.03.005

Combined NMR and Computational Study for Azide Binding to Human Manganese Superoxide Dismutase

Th. Emmler*[a+], I. Ayala[b], D. Silverman[b], S. Hafner[c], A. S. Galstyan[a], E.W. Knapp[a], G. Buntkowsky*[d]

[a] Institut für Chemie und Biochemie, Freie Universität Berlin, Takustraße 3,6 D-14195 Berlin, Germany. (+) Present address: GKSS Forschungszentrum Geesthacht GmbH, Max-Planck.Str. 1, D-21502 Geesthacht

[b] University of Florida, Gainesville, USA

[c] Varian Deutschland GmbH, Darmstadt

[d] Friedrich-Schiller-Universität, Jena, Institut für Physikalische Chemie, Helmholtzweg 4, D-07743 Jena, email: gerd.buntkowsky@uni-jena.de.

* Correspondence to: Gerd Buntkowsky, Friedrich-Schiller-Universität, Jena, Institut für Physikalische Chemie, Helmholtzweg 4, D-07743 Jena, email: gerd.buntkowsky@uni-jena.de

Keywords: Mangenese Super Oxide Dismutase, Azide, Solid State NMR, REDOR, Substrate Binding; ^{19}F-NMR; MnSOD

Abstract

Human manganese superoxide dismutase (MnSOD) labeled with 3-fluorotyrosine (Tyf) was complexed with the ^{15}N-labeled inhibitor azide ($[^{15}N_3^-]$). The sample was characterized by solid state NMR spectroscopy (^{19}F-MAS and ^{15}N-CPMAS). Employing ^{19}F-^{15}N-REDOR spectroscopy, we determined the distances between the fluorine label in Tyrosine-34 and the three ^{15}N-nuclei of the azide and the relative orientation of the azide in the binding pocket of the MnSOD. A distance of $R_1 = 4.85$ Å between the ^{19}F-label of Tyf34 and the nearest ^{15}N of the azide and an azide-fluorotyrosine Tyf34 angle of 90° were determined. These geometry data are employed as input for molecular modeling of the location of the inhibitor in the active site of the enzyme. In the computations, several possible binding geometries of the azide near the Mn-complex were assumed. Only when the azide replaces the water ligand at the Mn-complex we obtained a geometry of the azide Mn-complex, which is consistent with the present NMR data. This indicates that the water molecule ligating to the Mn-complex is removed and the azide is placed at this position. As a consequence the azide forms an H bond with Gln143 instead with Tyf34, in contrast to non-^{19}F labeled MnSOD, where the azide is hydrogen bonded to the hydroxy group of Tyr34.

Introduction

In course of aerobic metabolism, reduced forms of dioxygen, the superoxide radical anion (O_2^-) and hydrogen peroxide (H_2O_2), are generated mostly in mitochondria. These are cytotoxic, attacking for instance the unsaturated fatty acid components of the membrane lipids and DNA. Mitochondrial manganese superoxide dismutase (MnSOD) appears to be responsible to protect these organelles and other components of the cell from oxidative damage by catalyzing the decay of superoxide[1-7]. The protection of aerobic cells against superoxide and peroxide occurs in two subsequent reactions and involves two different enzymes, where O_2^- is completely reduced to non-toxic products:

$$2O_2^- + 2H^+ \xrightarrow{\text{superoxid dismutase}} H_2O_2 + O_2$$

$$2H_2O_2 \xrightarrow{\text{catalase}} 2H_2O + O_2$$

In the first reaction the superoxide radical is converted by superoxide dismutase (SOD) into hydrogen peroxide and oxygen; in the second reaction the peroxide is converted by catalase to oxygen and water. SODs can be divided into different classes depending on the metal complex used for catalysis: Manganese- and iron-containing SODs are very similar in structure and catalytic mechanism.[8-11] They are found in prokaryotes (Mn, Fe), in mitochondria (Mn), and in plants (Fe). In humans MnSOD is a homotetramer of four identical SOD units with a molecular weight of 22kD per monomer. SODs carry out catalysis by cycling through different oxidation states of the metal complex: Fe(III,II) or Mn(III,II). The scheme below shows a simple mechanism for the conversion of superoxide to peroxide that pertains to SODs.[12; 13]

$$Mn(III)SOD + O_2^- \rightarrow Mn(II)SOD + O_2 \quad \text{(Eq. 1)}$$
$$Mn(II)SOD + O_2^- + 2H^+ \rightarrow Mn(III)SOD + H_2O_2$$

The coordination geometry of the manganese complex in human MnSOD is trigonal bipyramidal, with three histidines, one monodentate aspartate, and one water as ligands.[14; 15] As it was shown in experimental[16] and theoretical studies,[17] the Mn water ligand is an anionic OH^- for the oxidized Mn-complex, which is protonated after reduction yielding neutral H_2O.

The catalytic activity of MnSOD is high ($k_{cat}/K_m \approx 10^9\ M^{-1}s^{-1}$ i.e. near the limit of diffusion control).[18] The efficiency of the enzyme requires high substrate accessibility for the active site and an open and exchangeable coordination position at the Mn-complex to allow for possible inner sphere electron transfer and subsequent rapid protonation of the peroxide anion. The proposed reaction mechanism of Stallings et al.[12] assumes that an intermediate complex forms in which the O_2^- radical is a direct, inner sphere ligand of manganese. Because of the short-lived and transient nature of such an intermediate complex, it is difficult to directly support this hypothesis, for example by a crystal structure of the corresponding enzyme-substrate complex. Alternatively, a substrate analogue, which binds to the Mn-complex, can be used to gain information. In case of the MnSOD, the azide anion (N_3^-) is a suitable substrate analogue and inhibitor. It appears to bind weakly to human MnSOD with a binding constant of 2.2 mM.[19]

Crystal structures of FeSOD from *E. coli* at 1.8 Å (R = 0.186) resolution and of MnSOD from *T. thermophilus* at 1.8 Å (R = 0.179) resolution were measured by Lah et al.[20]. Both structures reveal an azide as sixth ligand bound at the metal in a distorted octahedral geometry. The positions of the distal azide nitrogen atoms differ in FeSOD and MnSOD. In the MnSOD crystal structure, the azide is found as direct ligand of manganese and forms a hydrogen bond with the hydroxyl group of Tyr34. The ligand-metal-ligand angles show different binding modes of azide in MnSOD. The different geometries of the metal-azide species suggest a reaction mechanism for SOD in which the metal alternates between five- and six-fold coordination. Because of the differences in azide binding mode between MnSOD and FeSOD, and a possible relationship between azide and substrate binding, these binding modes need to be more completely understood. In particular, it is not proven that azide always binds directly to manganese in MnSOD as discussed for MnSOD from *E. coli*.[21]

In recent years, the thermochromic character of the azide ligated Mn-complex in MnSOD became evident. Accordingly, at low temperatures the Mn-complex is six-fold coordinated, while at elevated temperatures (transition temperature at about 200 K) it converts to a five-fold coordinated form.[21; 22] Other data show the presence of six-fold coordinated MnSOD still at room temperature.[20] It was also suggested that either the ligand Asp167 or water is dissociating with increasing temperature.[21-23] More recently, the azide was shown[24] to dissociate from the Mn-complex at room temperature.

As discussed above one cannot completely clarify the azide binding mode to Mn from the MnSOD

crystal structures. To shed light on this problem we present an effective and jet simple method to study the azide binding to human MnSOD by solid state NMR spectroscopy.[25]

The ^{19}F-labeled enzyme that we used was a mutant of the human MnSOD employed in previous liquid state NMR studies by some of us,[26] in which all tyrosine residues except Tyr176 were replaced with 3-fluorotyrosine. Tyr176 was replaced with phenylalanine. Since the latter is far from the active site this should not influence our study (see materials section below). Wild-type human MnSOD contains nine tyrosine residues, one of which, Tyr34, is located in the active-site with its side chain oxygen at about 5 Å from manganese. The electron density maps of fluorinated human MnSOD obtained by X-ray crystallography reveal that all side chains of 3-fluorotyrosine-34 (in the following abbreviated as Tyf34) have the same conformations as in the wild-type structure.[27] Incorporation of 3-fluorotyrosine does not significantly alter the structure of the fluorinated human MnSOD (The root mean square (RMS) deviation for all 198 α-carbon atoms is 0.3 Å.) The hydrogen bond pattern extending from the Mn-bound water is maintained in the structure of the human MnSOD containing 3-fluorotyrosines (Figure 1).

There are two different solid state NMR (SSNMR) strategies to determine molecular or supramolecular structures, namely (i) correlation of different chemical shift tensors[28] or other anisotropic NMR interactions,[29] which directly yield torsion angles and (ii) NMR measurement of intramolecular distances via chemical shifts or dipolar interactions, which constrain possible torsion angle values.[30-39] In the present study we use the second strategy and we employ a simple and commercially available ^{15}N labeled substrate for the NMR measurements. The hetero-nuclear dipolar couplings between ^{19}F and ^{15}N spins are measured by REDOR NMR[40-42] using an ^{19}F-labeled mutant of human MnSOD with ^{15}N-labeled azide as substrate. The dipolar couplings (the specification 'hetero-nuclear' is omitted from now on) are converted into internuclear distances and the supramolecular arrangement is adjusted to match these distances. Another (much more demanding) possibility to measure ^{19}F ^{15}N couplings is an additional high enrichment of the sample with ^{13}C. This allows the use of specialized 2D REDOR sequences (e.g. FRESH) [43] to obtain site specific information.

For the geometry determination the selection of the optimal azide isotopomers is crucial. The following points have to be considered: (i) the labeling scheme should give an unambiguous structure; (ii) the number of necessary isotopomers should be minimized; (iii) the chemical synthesis should be easy and cost efficient; (iv) the measured dipolar couplings should be in a range, where the REDOR experiments exhibit high sensitivity and yield accurate distances and (v) the often time consuming synthetical efforts for the substrate should be minimized. There are numerous papers that deal with the direct and indirect determination of torsion angles by high resolution solid state NMR (see for example refs. [44-52]), but owing to the considerations mentioned above we choose a ^{19}F/^{15}N-REDOR

experiment, employing fully ^{15}N-labeled azide (commercially available) and observing the ^{19}F nucleus while dephasing via the ^{15}N-nuclei. In this way up to three different dipolar couplings between the ^{19}F label and the ^{15}N-labels of the azide anion can be measured on a single sample and converted into distances. The drawback of this method is that the complex spin system necessitates an elaborate evaluation of the resulting REDOR data, as will be discussed in the results section in more detail. If the individual dipolar couplings are sufficiently strong, this evaluation can be solved by the so-called REDOR transform[53; 54]. Alternatively, full simulation of the experimental spin system can be performed[55-57] or specialized REDOR sequences like REDOR 3D,[58] FDR-REDOR,[59; 60] θ-REDOR,[61] or MS REDOR[62] can be employed. However, the latter procedure goes along with substantially longer measuring times.

The rest of the paper is organized as follows. First, a description of our experimental setup is given, followed by a brief survey of sample preparation and characterization and an overview about computational methods and calculations. Subsequently, the experimental results are presented, discussed and finally summarized.

Methods

Solid State NMR Spectroscopy

All solid state NMR measurements were performed at room temperature on commercial Varian InfinityPlus 500 and 600MHz NMR spectrometers operating at fields of 11.7 and 14 T.

For the heteronuclear distance measurements a variant of the REDOR[40] experiment was chosen, where the REDOR spectra were recorded after applying the recoupling pulses in the non-observed (dephasing) channel and the echo pulse in the observe channel was given in the center of the sequence. The recoupling pulses were phase cycled according to the xy-4 or xy-8 phase scheme.[63-65] Owing to the high molecular mass of the enzyme the signal of the samples was very low and the measurement of each spectrum took about 2 days.The 14 T ^{19}F/^{15}N-REDOR measurements were performed on a home built four channel 4mm H-XYZ transmission line probe (Schaefer/McKay type) and a commercial Varian 4mm HX T3 probe, where we modified the proton channel for fluorine observation. These experiments were done without proton decoupling. Resonance frequencies are 599.97 MHz for ^{1}H, 564.45 MHz for ^{19}F and 60.79 MHz for ^{15}N. In all REDOR-experiments the ^{19}F-nuclei were observed and all dephasing pulses were irradiated in the ^{15}N-channel. The frequency offset of the non observed (^{15}N) channel was set to 140ppm (between the two ^{15}N resonances of the Azide). Owing to sample degradation we could measure only at two dephasing times.

^{15}N-CP-MAS spectra were recorded at 14 T. Residual ^{1}HX dipolar couplings were suppressed using TPPM decoupling[66] with a B_1 field of 50 kHz. Ramped amplitude cross-polarization (RAMP-CP)[67] was used to enhance the CP efficiency at high spinning rates. Referencing of the CP-MAS spectra to NH_3 was performed employing $^{15}NH_4Cl$ as external standard. The sample spinning

frequency for all measurements was adjusted in the range of 1 to 10 kHz and was stabilized to about ±2 Hz. Typical π pulse lengths on all systems were 4.0 μsec for the ^{1}H channel, 5.0 μsec for the ^{19}F channel and 8.2 μsec for the ^{15}N channel. Typical recycle delays for the REDOR and CP/MAS measurements were 2.5s and 3s for the ^{19}F measurements 3s. The lyophilized sample (total amount was 10mg) was packed into a zirconium oxide rotor (see below for sample preparation). Proton decoupled ^{19}F-MAS spectra were recorded at 11.7 T employing a commercial 4mm Varian HF-XY. Resonance frequencies are 498.97 MHz for ^{1}H and 469.43 MHz for ^{19}F.

Data evaluation of REDOR experiments

The basic theory of the REDOR experiment for two-spin[40; 41; 68-70] and three-spin systems[55; 71] is well-known from literature and was implemented in laboratory written MATLAB scripts. The use of completely labeled Azide provides the possibility to measure three different couplings in one REDOR measurement (see figure 2). The azide ion is a linear, rigid molecule with 1.18 Å distance between neighbor nitrogen atoms. Its arrangement in the active site of the enzyme can be characterized with two parameters, namely by the distance from the Tyf34 ^{19}F to the proximal azide nitrogen and the angle between the azide axis and the distance vector from the Tyf34-fluorine to the proximal azide nitrogen (R1, see Figure 3). The REDOR decay curves have to be calculated employing a spin system of the IS_3 type, which includes not only heteronuclear $^{19}F/^{15}N$-couplings, but also homonuclear $^{15}N/^{15}N$ couplings between the dephasing S spins. To test, whether these couplings influence the REDOR signal, numerical simulations with laboratory written MATLAB routines and the SIMPSON program package[72] were performed employing the direct method in conjunction with the REPULSION set of 100 angles.[73] These simulations showed that the effect of the homonuclear ^{15}N-couplings on the dephasing of the ^{19}F-nucleus is negligible in our experiments. Therefore, the final fitting of the REDOR curves was done employing a laboratory written MATLAB routine, which uses purely heteronuclear $^{19}F/^{15}N$-couplings.

To study azide binding at the active site of MnSOD, ^{15}N-labeled azide was used. A direct detection of azide ^{15}N was only partially feasible, since the azide signal overlaps with the backbone ^{15}N signal (see Figure 5) and only the spinning side bands are clearly visible, which however are of low intensity. Accordingly, all distance determinations were done by a $^{19}F/^{15}N$-REDOR experiment, where the dephasing of the ^{19}F-MAS NMR echo spectra of Tyf34 is observed under the influence of dipolar couplings to $^{15}N_3^-$. In order to obtain a ^{19}F free background the spacers used for the filling of the rotor were made of Vespel® .

MnSOD Sample and Preparation

The fluorinated human MnSOD investigated was expressed in *E. coli* grown in minimal media supplemented with 3-fluorotyrosine.[27] Purification was performed by standard procedures.[27] The

wild-type human MnSOD contains nine Tyr residues. For our measurements, we used a mutant of human MnSOD where Tyr 176 was replaced by phenylalanine and nominally all other tyrosines are replaced by 3-fluorotyrosine. This mutant was previously employed in a ^{19}F liquid state NMR study of MnSOD.[26] Phe176 is at about 9 Å from Mn. Replacement of Tyr176 by Phe caused no change in the NMR spectrum of the remaining ^{19}F resonances.[26] The Mn content in MnSOD was determined using flame atomic absorption spectroscopy yielding 80% of active sites occupied by manganese. Typically in our procedures fluorotyrosine is incorporated into about 75% of all tyrosine sites in human MnSOD, determined by amino acid analysis and by MALDI-TOF mass spectrometry

The MnSOD sample used for the measurements was prepared from a lyophilized solution colored slightly violet from which the solvent was subsequently evaporated at room temperature. It contained equimolar amounts of azide and MnSOD monomers (human MnSOD containing 3-fluorotyrosine). In solution the sample had a maximal absorbance at 480 nm indicating that MnSOD was predominantly in the oxidized state Mn(III)SOD.

Computational Methods

In order to model the azide bound to the Mn-complex in MnSOD we used the crystal structure of human MnSOD with fluorinated tyrosines, which is available at high resolution of 1.85 Å.[74] The MnSOD crystal structure consists in two monomers per unit cell (chain A and chain B) with RMS deviation between these two chains of around 1.43 Å (without hydrogen atoms). We arbitrarily took the atomic coordinates from chain A. Since hydrogen atoms are missing in the crystal structure, we generated them using H-build from CHARMM27[75] that adds hydrogens according to topological information, followed by geometry optimization of hydrogen atom positions while the crystallographic coordinates of all other atoms were fixed.

Quantum-chemical computations were performed with the DFT B3LYP functional[76-79] as implemented in Jaguar version 5. The Mn-complex models were geometry optimized in vacuum by quantum chemical energy minimization using LACVP basis set and effective core potential for Mn[80] and 6-31G basis functions for the other atoms. In total, we performed three series (I, II, III) of geometry optimizations with different geometric constraints as explained below.

Series I and II. In series I and II the model structure of the azide-Mn-complex was generated by inserting the azide molecule as a sixth ligand into the MnSOD active center of the crystal structure[74] using the azide related structural information of the MnSOD crystal structure from *T. thermophilus*.[20] Our model of the Mn-complex includes the residues His26, His74, His163, Asp159, H_2O/OH^-(MW1) belonging to the first ligand-sphere, as well as Gln143 and Tyf34 from the second ligand-sphere (Figure 3). Although polypeptide backbone atoms were excluded from the model, the C_α atoms of the considered residues were used as virtual atoms X_α to stabilize the residue conformations during geometry optimization. Additionally, for Gln143 the -$C_\beta H_2$- group was truncated, while the C_β atom was used as virtual atom X_β. Aliphatic groups were truncated by substituting them by hydrogen

atoms H_T.

Figure 3:

We consider the Mn-complex in the oxidation states Mn^{2+} and Mn^{3+}. In both oxidation states the MnSOD was found to be in the high spin state.[81] Therefore, we used total spin of S=2 and S=5/2 for the Mn^{2+} and Mn^{3+} redox states, respectively. The series I and II computations differ in degree and character of the geometric constraints used for the quantum chemical energy minimization. While in series I the constraints reflect implicitly the presence of the protein environment that restricts the mobility of the Mn-complex ligands drastically, constraints in series II allow for structural relaxation to a larger extent. In this way it is possible to indirectly see how the protein matrix constrains the Mn-complex geometry.

In series I the following constraints were applied during geometry optimization: We fixed (i) the His26, His74 and His163 C_β and C_γ atom positions and the corresponding dihedral angles X_α-C_β-C_γ-N_δ; (ii) the Asp159 C_β atom position and the corresponding dihedral angle X_α-C_β-C_γ-O_δ, (iii) the Gln143 C_γ atom position and the corresponding dihedral angle X_β-C_γ-C_δ-O_ε, (iv) the Tyf34 C_β, C_γ, $C_{\delta1}$, $C_{\delta2}$, $C_{\varepsilon1}$, $C_{\varepsilon2}$ and C_ζ atoms. Additionally, all H_T hydrogens and virtual atoms were fixed. In series II only those dihedral angles were fixed, which do not include hydrogens, azide nitrogen atoms or virtual atoms (see the input files in Table S1 and S2 of supporting information).

Series III. The series III computations were performed by combining the CHARMM[75] classical force field and quantum chemical DFT methods. In this case, we considered the modeled hypothetical five-fold coordinated azide-Mn^{3+}-complex, where the solvent ligand is substituted by an azide-anion. First, azides were inserted in both MnSOD monomers of the crystal structure of human MnSOD with fluorinated tyrosines[74] such that the coordinating azide nitrogens were placed on the positions of the water ligand oxygens at a distance of 4.2Å between F_{Tyf34} and the N_{azide} proximal to Mn and F_{Tyf34}. Subsequently, these azides were oriented to yield ϑ angles of ~90°. For a definition of the angle ϑ see Fig. 3 below. As will be shown in the Results section, the proximal N_{azid} to F_{Tyf34} distance was determined experimentally to be ~4.85Å, and the ϑ angle to be ~90°. These initial azide conformations in the MnSOD crystal structure are energetically unfavorable because of steric clashes, unless the protein environment is able to relax. For that reason the MnSOD structure of both monomers was fully optimized using the CHARMM force field, while all crystal waters were removed to leave more space for relaxation of the protein structure. For the residues considered in this geometry optimization the RMS deviation between the MnSOD structures before and after minimization is about 1Å.

Although usage of a classical force field is important to obtain a relaxed protein structure, however, it may be insufficient to treat the Mn-complex appropriately. The force field cannot describe the σ-/π-bonding of Mn–ligand interactions. Therefore, it is necessary to geometry optimize the Mn-complex

furthermore by quantum chemical methods. For this purpose, we arbitrarily took the atomic coordinates from chain A of the dimeric MnSOD crystal structure. The corresponding starting structure for DFT calculations of the Mn-complex in MnSOD includes from the first coordination sphere the ligands azide, His26, His74, His163, Asp159 and from the second coordination sphere Tyf34, Gln143, Trp123, Trp161. Like in the series I and II models the backbone atoms were substituted by X_α virtual atoms placed on the C_α positions. Only in case of Trp161 $C_\alpha H$ and $-NH_2$ from the polypeptide backbone were considered explicitly because of hydrogen bond possibilities between NH_2 and Asp159. Here, the carbonyl atom of the Trp161 backbone was exchanged by a virtual atom X. Truncated molecular groups were substituted by H_T hydrogen atoms. We considered the oxidized form of the azide Mn^{3+}SOD complex in the high spin state (S=2). The starting structure was optimized quantum chemically using the following constraints: (i) in first ligand sphere all X_α-C_β bond lengths and X_α-C_β-C_γ bond angles were fixed, (ii) in the second ligand sphere the positions of all C_β and for Trp161 also the Cγ atom were fixed (see input file in Table S5 of supporting information).

Results

^{19}F MAS and ^{15}N-CPMAS spectra

Figure 4 shows the ^{15}N-MAS NMR spectra of pure sodium azide, and azide in the presence of MnSOD. In pure sodium azide, the outer nitrogens resonate at 60 ppm and the central nitrogen at 220 ppm. In MnSOD the central azide nitrogen overlaps with the natural abundance MnSOD signal. The shift of the outer nitrogen resonance lines indicates the closeness of the azide to the paramagnetic Mn, which also broadens the ^{15}N-resonances of the azide.

Figure 5 displays the proton decoupled ^{19}F MAS spectra of solid MnSOD directly after a 90° pulse and after 2msec echo delay time. The spectra of the tyrosine residues show under ^{1}H-decoupling a broad and a relatively narrow component. The broad signal is rather weak and low-field shifted. Without ^{1}H-decoupling, both components collapse to a single unresolved line. In principle, these two components could result either from structural inhomogeneities in the sample, i.e., a coexistence of crystalline (narrow) and disordered parts or from a pseudo contact shift caused by the influence of the paramagnetic Mn[82].

The chemical shift difference of the two lines is about 10 ppm and due to the broadening of the line we attribute the low field part of this line to the ^{19}F of Tyf34 in the vicinity of the paramagnetic Mn. The other component is attributed to the remaining Tyf residues (Tyf45, Tyf 193, Tyf 11, Tyf 169 and Tyf

166). Comparing the line intensities of the FID spectrum with the 2msec and 5msec echo spectra (the latter is not shown) reveals that the broad component has a significantly longer T_2.

REDOR distance measurements

In the following the results of the $^{19}F/^{15}N$-REDOR distance measurements are presented. Figure 6 compares the reference and the REDOR spectrum of the $^{19}F/^{15}N$-REDOR measurement after 3msec dephasing time. Compared to figure 5 it seems that the sideband at 30ppm is only poorly visible. As it is evident in figure 5 the sideband at 30ppm is already smaller than the next sideband close to 50ppm. This leads in the undecoupled echo spectra to a poorly visible signal.

The REDOR distance data (due to the absence of chemical shift resolution since all signals collapse into a single one when no ^1H decoupling is applied) were obtained in a set of experiments, where the ^{19}F-nuclei were observed without ^1H-decoupling. While these experiments have the disadvantage of lower resolution in the ^{19}F-spectra, they are easy to do with standard solid state MAS NMR hardware and their interpretation does not depend on the line shape analysis of the ^{19}F-spectra. Since all fluorine lines overlap in this case, the achievable maximum dephasing is given by the stoichiometry of the sample as nominally 12.5%. The integral of the largest signal close to 17ppm, which has the best S/N ratio, was used for the data analysis. Tests where all side bands were integrated did not give significant differences in the dephasing.

Discussion

For the interpretation of the REDOR spectra, it was necessary to calculate the influence of ^{19}F in 3-fluorotyrosine Tyf34 on dephasing caused by the simultaneous presence of the three ^{15}N azide spins. Since the N-N bond length of the linear azide is known (1.18A), it is possible to calculate the individual distances of Tyf34–^{19}F to all three azide ^{15}N atoms, using the distance between Tyf34–^{19}F to the closest azide ^{15}N and the angle ϑ as defined in Figure 2.

From the resulting diagram (Figure 7), not only the distance but also the relative orientation of the molecular axis of the azide to the ^{19}F-^{15}N-vector is determined. The best fits were obtained for a distance of R_1 = 4.85 Å and an azide-fluorotyrosine Tyf34 angle of 90° (solid line in Figure 7), which describes the relative orientation of the azide in the binding pocket of the MnSOD. For the determination of the errors of this distance the stoichiometry of the sample is important. The 75% fluorotyrosine labeling (see MnSOD sample and preparation) doesn't influence the results of our investigation, since the ^{19}F spectra of fluorotyrosines are observed and the normal tyrosine molecules do not contribute to our results. The 10% error occupancy of the Mn ions however causes a systematic error in the resulting data and has to be taken into account, since the lack of Mn leads to a different hydrogen bonding pattern in the active site so that probably no

azide is bond there. To estimate the overall error we varied the parameters of our simulations and took those parameters which are still compatible (figure 7) to our data as a measure for the accuracy of the distance and angles.

The results obtained by the $^{19}F/^{15}N$ REDOR measurements and comparisons of the CPMAS spectra of the human MnSOD with azide as inhibitor and the Na azide results are pointing to a relatively close proximity of azide to Mn. The center azide nitrogen is about 5 Å from the ^{19}F of the 3-fluorotyrosine Tyf34. The distance between ^{19}F-Tyf34 and Mn is about 4.2 Å, which is much longer than that in the MnSOD crystal structure from *T. thermophilus* of Lah et al.[20], where azide is ligated to Mn in close proximity to Tyr36, equivalent to Tyf34 in human MnSOD. The reason for this difference could be the steric hindrance from the fluorine atom on the meta-position of Tyf34 carrying a partial negative charge of about -0.15 and being relatively voluminous compared to hydrogen. This would also be a possible explanation of the fact that in contrast to NMR-spectra, the crystal structure of human MnSOD with fluorinated tyrosines[74] does not possess azide. In contrast to the NMR-spectra measured at room temperature, the crystal structure was sampled at low temperatures of 100K where the MnSOD structure should be more compact than at room temperature. Such temperature dependent volume changes were for instance observed in RNase A.[83] These volume reductions increase steric and electrostatic influences between the Tyf34 fluorine atom with its partial negative charge and the azide-anion, which may prevent azide binding to the Mn-complex. The dependence of energetics and kinetics of azide-ligand binding/dissociating to/from the Mn-complex in MnSOD on ligands of the second shell such as Tyr34 was recently discussed[24] supporting our assumptions. Moreover, our constrained DFT calculations series I and II on the modeled azide-Mn-complex show, that the azide ligand can dissociate or bind dependent on steric factors (see Figure S1 and S2 of supporting information). While in the relatively relaxed conformation of series II calculations the modeled azide molecule remains ligated, in the more constrained series I case the azide dissociates from the Mn-complex remaining H-bonded to Tyf34. From these results it is obvious that the structural changes in protein environment are able to influence the process to coordinate azide to the Mn-complex. Recently,[24] combining experimental and computational data, a temperature dependent dynamical equilibrium was found for the active site in MnSOD crystals from *Escherichia coli*, where at low temperatures the azide-anion is coordinated to the Mn-complex as sixth ligand, while at room temperature it dissociates from the Mn-complex, but remains H-bonded to Tyr34. According to our NMR data at room temperature we can conclude that azide is H bonded neither to Tyf34 nor to His30, since this would result in N_{azid}-F_{Tyf34} distances smaller than 4 Å. Alternatively, the azide might be located in the water funnel where it forms H bonds with water, but this likely leads to disordered conformations, with no definite geometry. Surprisingly, the solution of this puzzle seems to be that at room temperature the azide substitutes the water (H_2O/OH^-) ligand at the Mn-complex. The computations of series III show that placing azide at the position of the water ligand the geometric

data derived from NMR-spectra can be reconciled (Fig. 8).

Summary and Conclusion

The present study shows that dipolar solid state NMR spectroscopy is a valuable tool for functional studies of large biomolecules such as MnSOD. Employing a well-chosen isotope-labeling scheme it is possible to determine the distance and relative orientation of the azide inhibitor inside the active site of MnSOD with very high precision. These distance data can be employed as input to determine by molecular modeling the exact position of the inhibitor in the active center of MnSOD.

The agreement of the data recorded without ^{1}H decoupling shows that even complicated ^{19}F-X REDOR measurements like the one presented here can be made with a standard HX probe and so can be applied routinely. It was shown that a maximum dephasing of around 12% is enough to interpret REDOR data without chemical shift resolution even in complicated systems like enzymes. The detection of ^{19}F instead of ^{15}N results in a background free spectra that are not disturbed by any natural abundance nuclei (like the ^{15}N in the enzyme's backbone that overlap with the signal from the Azide used in this study). However experimental factors like the QF of the probes and limited measurement time show the necessity to employ computational methods as part of the shown strategy.

To fully locate the azide inside the active center, a second, independent distance vector is necessary. In principle such a vector could be provided by dipolar interaction to the manganese ion. In practice however, this is not feasible due to the paramagnetic nature of Mn, which shortens T_2 relaxation times exceedingly. Instead, we propose to employ the paramagnetic center itself as source of additional structural constraints for the location of the substrate. For this purpose the spin-relaxation and paramagnetic shifts of the ^{15}N-, ^{13}C- and ^{19}F-labels in the active site have to be analyzed in detail and compared to calculations and experimental data on a set of reference components, for example simple manganese complexes with known structure, to calibrate these data.

The calculations predict three different arrangements of the manganese azide complex (series I, II and III), depending on the amount of structural relaxation allowed for the protein environment. In two of these arrangements (I and II) the azide is hydrogen bonded to the Tyf34 and in configuration II, which allows for the relaxation of backbone atoms of the side chains ligated to the manganese, the azide is also coordinated to the manganese ion. However these configurations are only in poor agreement with NMR data. A much better agreement between NMR data and calculations is found in configuration III, where the azide is assumed to replace the water ligand at the Mn-complex.

In the computations, several possible binding geometries of the azide near the Mn-complex were assumed. Only when the azide replaces the water ligand at the Mn-complex we obtained an azide Mn-complex geometry, which is consistent with the present NMR data. This gives rise to a number of

interesting questions. Obviously the replacement of Tyr34 by the fluorinated Tyf34 disfavors azide to ligate the Mn-complex at the side of this Tyrosine. Furthermore, the water content of the MnSOD sample may be an important factor to determine the azide binding site. As long as a water molecule (MW1 in Figure 1) is coordinated to the Mn-complex, the azide can only be placed on the Tyf34 side and forms an H bond to Tyf34. Depending on weak or strong constraining conditions of the ligand environment, corresponding to computations of series II and I, azide may be ligated or not ligated to the Mn-complex, respectively. If the water molecule MW1 ligated to the Mn-complex is removed the azide can be placed at this position. As a consequence the azide forms an H bond with Gln143 instead of Tyf34, corresponding to the computation of series III (Figure 8). This raises the question whether the location of the azide may be directly connected to the water content of the MnSOD sample, which in general is higher in crystallized samples than in lyophilized samples or, whether the replacement of Tyr34 by Tyf34 is sufficient to enable the azide to drive the water away from the manganese ion. In principle this question could be answered by further NMR measurements on microcrystalline samples.

Acknowledgements

This work was supported by the Deutsche Forschungsgemeinschaft DFG and National Institute of Health under grant NIH GM 54903. The authors wish to thank J. Perry, Scribbs for providing us with the X-ray structure of the MnSOD before publication, Dr. Martin Karplus for providing the program CHARMM.

References

[1] J.M. McCord, and I. Fridovich, J. Biol. Chem. 244 (1969) 6049-6055.
[2] J.M. McCord, J. Keele, B. B., and I. Fridovich, Proc. Nat. Soc. USA 68 (1971) 1024-1027.
[3] I. Fridovich, Annu. Rev. Biochem. 44 (1975) 147-159.
[4] B.B. Keele, Jr., McCord, J. M., Fridovich, I., J. Biol. Chem. 245 (1970) 6176-6181.
[5] J.L. Hsu, Hsieh, Y., Tu, C., O'Connor, D., Nick, H.S., Silverman, D.N., J. Biol. Chem. 271 (1996) 17687–17691.
[6] J.M. McCord, Boyle, J. A., Day, E. D., Jr., Rizzolo, L. J., Salin, M. L., Superoxide and Superoxide Dismutases, Academic, New York, 1977.
[7] I. Fridovich, J. Biol. Chem. 264 (1989) 7761-7764.
[8] A.-F. Miller, and D.L. Sorkin, Comments Mol. Cell. Biophys. 9 (1997) 1-48.
[9] B. Meier, C. Scherk, M. Schmidt, and F. Parak, Biochem. J. 331 (1998) 403-407.
[10] M. Schmidt, B. Meier, C. Scherk, O. Iakovleva, and F. Parak, Prog Biophys Mol Bio 65 (1996) Pa113-Pa113.
[11] M. Schmidt, B. Meier, and F. Parak, J Biol Inorg Chem 1 (1996) 532-541.
[12] W.C. Stallings, C. Bull, J.A. Fee, M.S. Lah, and M.L. Ludwig, In Molecular Biology of Free Radical Scavenging Systems, Cold Spring Harbor Laboratory Press, Plainview, NY, 1992.
[13] A.F. Miller, Fe superoxide dismutase. in: R.H. Albrecht Messerschmidt, Thomas Poulos and Karl Wieghardt, (Ed.), Handbook of Metalloproteins, John Wiley & Sons, Chichester, 2001.
[14] R.H. Holm, Kennepohl, P., Solomon, E.I., Chem. Rev. 96 (1996) 2239-2314.
[15] G.E.O. Borgstahl, H.E. Parge, M.J. Hickey, W.F. Beyer, R.A. Hallewell, and J.A. Tainer, Cell 71 (1992) 107-118.

[16] A.F. Miller, K. Padmakumar, D.L. Sorkin, A. Karapetian, and C.K. Vance, J. Inorg. Biochem. 93 (2003) 71-83.
[17] W.G. Han, T. Lovell, and L. Noodleman, Inorg. Chem. 41 (2002) 205-218.
[18] M.E. McAdam, Fox, R. A., Lavelle, F., Fielden, E. M., Biochem. J. 165 (1977) 71.
[19] A.S. Hearn, Stroupe, M.E., Cabelli, D.E., Ramilo, C.A., Luba, J.P., Tainer, J.A., Nick, H.S., Silverman, D.S., Biochem. 42 (2003) 2781 - 2789.
[20] M.S. Lah, Dixon, M.M., Pattridge, K.A., Stallings, W.C., Fee, J.A., Ludwig, M.L., Biochemistry 34 (1995) 1646-1660.
[21] M.M. Whittaker, Whittaker, J.W., Biochemistry 35 (1996) 6762.
[22] M.M. Whittaker, and J.W. Whittaker, J Biol Inorg Chem 2 (1997) 667-671.
[23] J.W. Whittaker, J Phys Chem B 101 (1997) 674-677.
[24] T.A. Jackson, A. Karapetian, A.F. Miller, and T.C. Brunold, J. Am. Chem. Soc. 126 (2004) 12477-12491.
[25] K. Schmidt-Rohr, and H.W. Spiess, Multidimensional Solid State NMR and Polymers, Academic Press, London, 1994.
[26] P. Quint, I. Ayala, S.A. Busby, M.J. Chalmers, P.R. Griffin, J. Rocca, H.S. Nick, and D.N. Silverman, Biochemistry 45 (2006) 8209-8215.
[27] I. Ayala, J.J.P. Perry, J. Szczepanski, M.T. Vala, J.A. Tainer, H.S. Nick, and D.N. Silverman, Biophys. J. 89 (2005) 4171-4179.
[28] K. Schmidt-Rohr, J.Am.Chem.Soc. 118 (1996) 7601.
[29] G. Buntkowsky, I. Sack, H.-H. Limbach, B. Kling, and J. Fuhrhop, J.Phys.Chem.B 101 (1997) 11265.
[30] S. Macholl, I. Sack, H.-H. Limbach, J. Pauli, M. Kelly, and G. Buntkowsky, Magn. Reson. Chem. 38 (2000) 596.
[31] G. Facey, D. Gusev, S. Macholl, R.H. Morris, and G. Buntkowsky, Phys.Chem.Chem.Phys. 2 (2000) 935.
[32] S. Macholl, F. Boerner, and G. Buntkowsky, Chemistry 10 (2004) 4808 - 4816.
[33] I. Sack, Y.S. Balazs, S. Rahimipour, and S. Vega, J. Magn. Reson. 148 (2001) 104-114.
[34] I. Sack, Y.S. Balazs, S. Rahimipour, and S. Vega, J. Am. Chem. Soc. 122 (2000) 12263.
[35] E. Hughes, T. Gullion, A. Goldbourt, S. Vega, and A.J. Vega, J. Magn. Reson. 156 (2002) 230-241.
[36] E. Hughes, J. Jordan, and T. Gullion, J Phys Chem B 105 (2001) 5887-5891.
[37] G. Goobes, and S. Vega, J. Magn. Reson. 154 (2002) 236-251.
[38] A. Goldbourt, S. Vega, T. Gullion, and A.J. Vega, J. Am. Chem. Soc. 125 (2003) 11194-11195.
[39] T. Emmler, S. Gieschler, H.H. Limbach, and G. Buntkowsky, J.Mol.Struct. (2004) 29-38.
[40] T. Gullion, and J. Schaefer, J.Magn.Res. 81 (1989) 196.
[41] T. Gullion, and J. Schaefer, Adv. in Magn. and Opt. Res. Ed.W.S. Warren 13 (1989) 57.
[42] V. Schimming, C.G. Hoelger, G. Buntkowsky, I. Sack, J.H. Fuhrhop, S. Rocchetti, and H.-H. Limbach, J.Am.Chem.Soc. 121 (1999) 4892.
[43] D.T. Graesser, B.J. Wylie, A.J. Nieuwkoop, W.T. Franks, and C.M. Rienstra, Magn. Reson. Chem. 45 (2007) 129-134.
[44] X. Feng, Y.K. Lee, D. Sandstrom, M. Eden, H. Mausel, A. Sebald, and M.H. Levitt, Chem.Phys.Lett. 257 (1996) 314.
[45] X. Feng, P.J.E. Verdegem, Y.K. Lee, D. Sandström, M. Eden, P. Bovee-Geurts, W.J. deGrip, J. Lugtenburg, H.J.M. deGroot, and M.H. Levitt, J.Am.Chem.Soc. 119 (1997) 6853.
[46] P.R. Costa, J.D. Gross, M. Hong, and R.G. Griffin, Chem. Phys. Lett. 280 (1997) 95-103.
[47] M. Hong, J. Gross, W. Hu, and R. Griffin, J. Magn. Res. 135 (1998) 169-177.
[48] C.M. Rienstra, M. Hohwy, L.J. Mueller, C.P. Jaroniec, B. Reif, and R.G. Griffin, J. Am. Chem. Soc. 124 (2002) 11908-11922.
[49] A.T. Petkova, G. Buntkowsky, F. Dyda, R.D. Leapman, W.-M. Yau, and R. Tycko, J.Mol.Bio. 335 (2004) 247-260.
[50] J.C.C. Chan, and R. Tycko, J. Am. Chem. Soc. 125 (2003) 11828-11829.
[51] R. Tycko, Curr. Opin. Struct. Biol. (2004) 96-103.
[52] C.P. Jaroniec, C.E. MacPhee, V.S. Bajaj, M.T. McMahon, C.M. Dobson, and R.G. Griffin, Proc. Natl. Acad. Sci. U. S. A. 101 (2004) 711-716.
[53] K.T. Mueller, T.P. Jarvie, D.J. Aurentz, and B.W. Roberts, Chem.Phys. Lett. 242 (1995) 535.

[54] J. d'Espinose de la Caillerie, and C. Fretigny, J.Magn. Res. 133 (1998) 273.
[55] J.M. Goetz, and J. Schaefer, J.Magn.Res 127 (1997) 147.
[56] C.A. Fyfe, A.R. Lewis, J.M. Chezeau, and H. Grondey, J. Am. Chem. Soc. 119 (1997) 12210-12222.
[57] M. Bertmer, and H. Eckert, Solid State NMR 15 (1999) 139.
[58] C.A. Michal, and L.W. Jelinski, J. Am. Chem. Soc. 119 (1997) 9059-9060.
[59] A.E. Bennett, L.R. Becerra, and R.G. Griffin, J. Chem. Phys. 100 (1994) 812.
[60] A.E. Bennett, C.M. Rienstra, P.T. Lansbury, and R.G. Griffin, J. Chem. Phys. 105 (1996) 10289.
[61] T. Gullion, and C. Pennington, CHEM PHYS LETT 290: (1-3) 88-93 (1998).
[62] O. Liivak, and D.B. Zax, J. Chem. Phys. 113 (2000) 1088-1096.
[63] T. Gullion, D.B. Baker, and M.S. Conradi, J.Magn.Res. 89 (1990) 479.
[64] T. Gullion, and J. Schaefer, J.Magn.Res. 92 (1991) 439.
[65] Y. Li, and J.N.S. Evans, J.Magn.Res.A. 116 (1995) 150.
[66] A.E. Bennett, C.M. Rienstra, M. Auger, K.V. Lakshmi, and R.G. Griffin, J.Chem.Phys. 103 (1995) 6951.
[67] G. Metz, X. Wu, and S.O. Smith, Journal of Magnetic Resonance A 110 (1994) 219-227.
[68] A.E. Bennett, R.G. Griffin, and S. Vega, Springer Series in NMR 33 (1994) 1.
[69] J. Garbow, and T. Gullion, Carbon-13 NMR Spectroscopy of Biological Solids, Academic Press Inc., New York, 1995.
[70] I. Sack, S. Macholl, J.H. Fuhrhop, and G. Buntkowsky, Phys.Chem.Chem.Phys. 2 (2000) 1781.
[71] A. Naito, K. Nishimura, S. Tuzi, and H. Saito, Chem. Phys. Let. 229 (1994) 506-511.
[72] M. Bak, J.T. Rasmussen, and N.C. Nielsen, J.Magn.Res. 147 (2000) 296.
[73] M. Bak, and N.C. Nielsen, J. Magn. Reson. 125 (1997) 132-139.
[74] A.T. Brunger, P.D. Adams, G.M. Clore, W.L. DeLano, P. Gros, R.W. Grosse-Kunstleve, J.S. Jiang, J. Kuszewski, M. Nilges, N.S. Pannu, R.J. Read, L.M. Rice, T. Simonson, and G.L. Warren, Acta Crystallogr D 54 (1998) 905-921.
[75] A.D. MacKerell, D. Bashford, M. Bellott, R.L. Dunbrack, J.D. Evanseck, M.J. Field, S. Fischer, J. Gao, H. Guo, S. Ha, D. Joseph-McCarthy, L. Kuchnir, K. Kuczera, F.T.K. Lau, C. Mattos, S. Michnick, T. Ngo, D.T. Nguyen, B. Prodhom, W.E. Reiher, B. Roux, M. Schlenkrich, J.C. Smith, R. Stote, J. Straub, M. Watanabe, J. Wiorkiewicz-Kuczera, D. Yin, and M. Karplus, J Phys Chem B 102 (1998) 3586-3616.
[76] J.C. Slater, Quantum theory of molecules and solids, McGraw-Hill, New York, 1974.
[77] S.H. Vosko, L. Wilk, and M. Nusair, Can. J. Phys. 58 (1980) 1200-1211.
[78] A.D. Becke, Phys. Rev. A 38 (1988) 3098-3100.
[79] C.T. Lee, W.T. Yang, and R.G. Parr, Phys Rev B 37 (1988) 785-789.
[80] P.J. Hay, and W.R. Wadt, J. Chem. Phys. 82 (1985) 299-310.
[81] J.W. Whittaker, Whittaker, M.M., J. Am. Chem. Soc. 113 (1991) 5528 - 5540.
[82] I. Bertini, and C. Luchinat, NMR of paramagnetic molecules in biological systems, Benjamin/Cummings Publ. Menlo Park, CA, 1987.
[83] L. Mitra, N. Smolin, R. Ravindra, C. Royer, and R. Winter, Phys Chem Chem Phys 8 (2006) 1249-1265.

Figure captions:

Figure 1:
Crystal structures of the active site environment of human MnSOD (adapted from ref.[27]). The wild-type MnSOD (green carbon atoms) is superimposed with 3-fluorotyrosine MnSOD (yellow carbon atoms with fluorine atoms in light blue) in which the nine tyrosine residues have been replaced. The apparent H-bond pattern (grey spheres) between the manganese-bound water MW1, side chains of Gln143, Tyr34, Tyr166, the crystal water HOH407 and His30 are conserved in both crystal structures.[27] The residues Tyr34 and His30 are located at the base of a solvent-access funnel, filled with water.

Figure 2:
Model for the Tyr34^{19}F–azide^{15}N geometry calculations.

Figure 3:
Starting structure of MnSOD active-site complex model with assembled azide ligand for series I and II computations. Except for azide, atomic coordinates of residues were taken from the crystal structure of human MnSOD.[74] For the sake of clarity hydrogen atoms were omitted in the figure except for the ligand water and the OH group of Tyf34. The dashed lines show hydrogen bonds.

Figure 4:
^{15}N-MAS NMR measurements of the Na$^{15}N_3$. Lower trace: ^{15}N-azide, 10 kHz, 1 pulse measurement. Upper trace: MnSOD complexed with the ^{15}N labeled azide, 5 kHz, VACP MAS measurement. We attribute the signal at 120ppm in the upper spectrum to a spinning sideband of the $^{15}N^-$ in the enzyme.

Figure 5:
^{1}H decoupled ^{19}F-MAS solid state NMR spectra (single pulse (lower trace) and echo) of human MnSOD. The broad component is attributed to the Tyf residues (see text) close to the paramagnetic manganese center.

Figure 6:
^{19}F reference (green trace) and dephased (red trace) spectra of MnSOD at 3 ms dephasing time.

Figure 7:
Best fit (solid line) for the orientation of azide compared to the ^{19}F-tyrosine plane (dephasing multiplied by 8 to get 1 as the final value). The dotted and dashed lines mark the error intervals.

Figure 8:
Optimized structure of azide Mn^{3+}-complex from series III computations. For the sake of clarity hydrogen atoms were omitted in the figure except for the ligand water and the OH group of Tyf34. The dashed lines show hydrogen bonds. The molecular model yields an N_{azid}-F_{Tyf34} R_1 distance of 4.75 Å (exp. ~4.85Å), and a ϑ angle of ~91° (exp. ~90°).

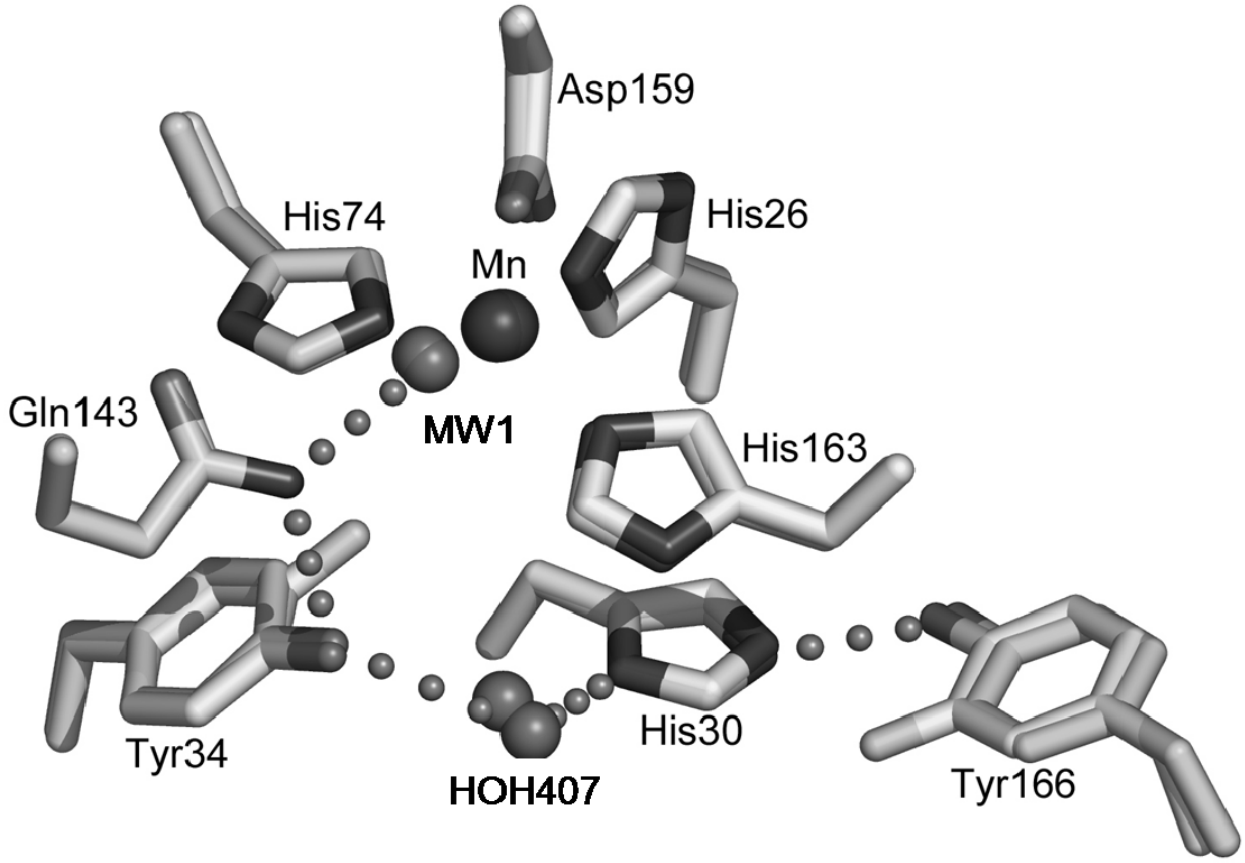
Asp159
His74
His26
Mn
MW1
Gln143
His163
Tyr34
His30
HOH407
Tyr166

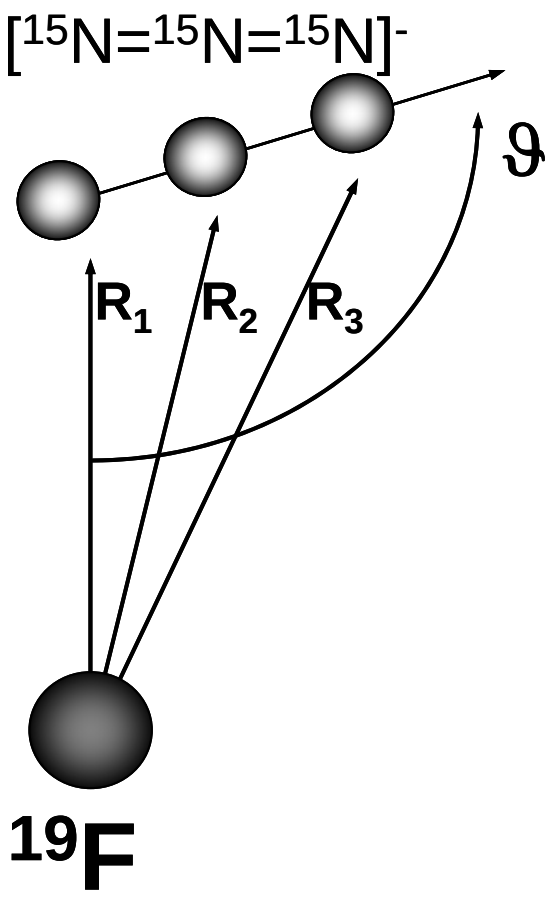
[15N=15N=15N]-
ϑ
R1
R2
R3
19F

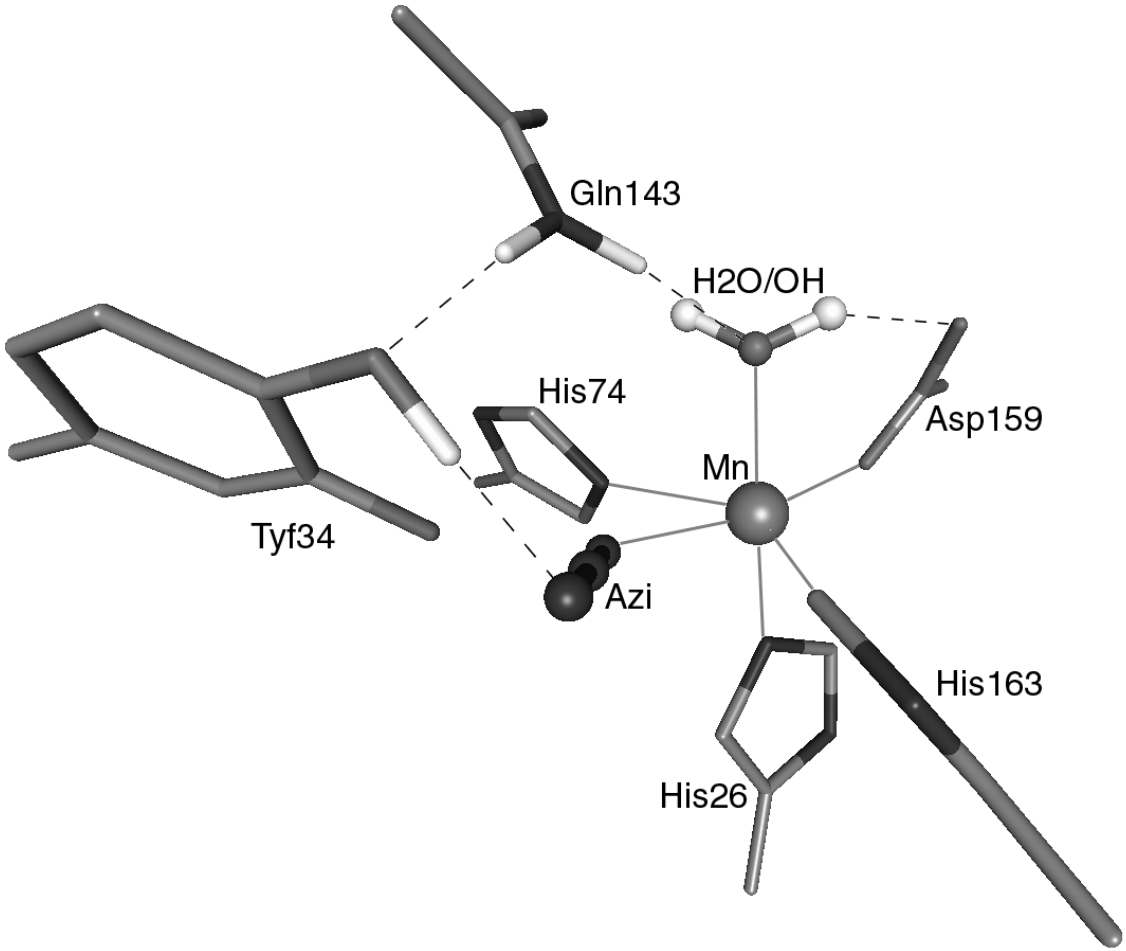
Gln143
H2O/OH
His74
Asp159
Mn
Tyf34
Azi
His163
His26

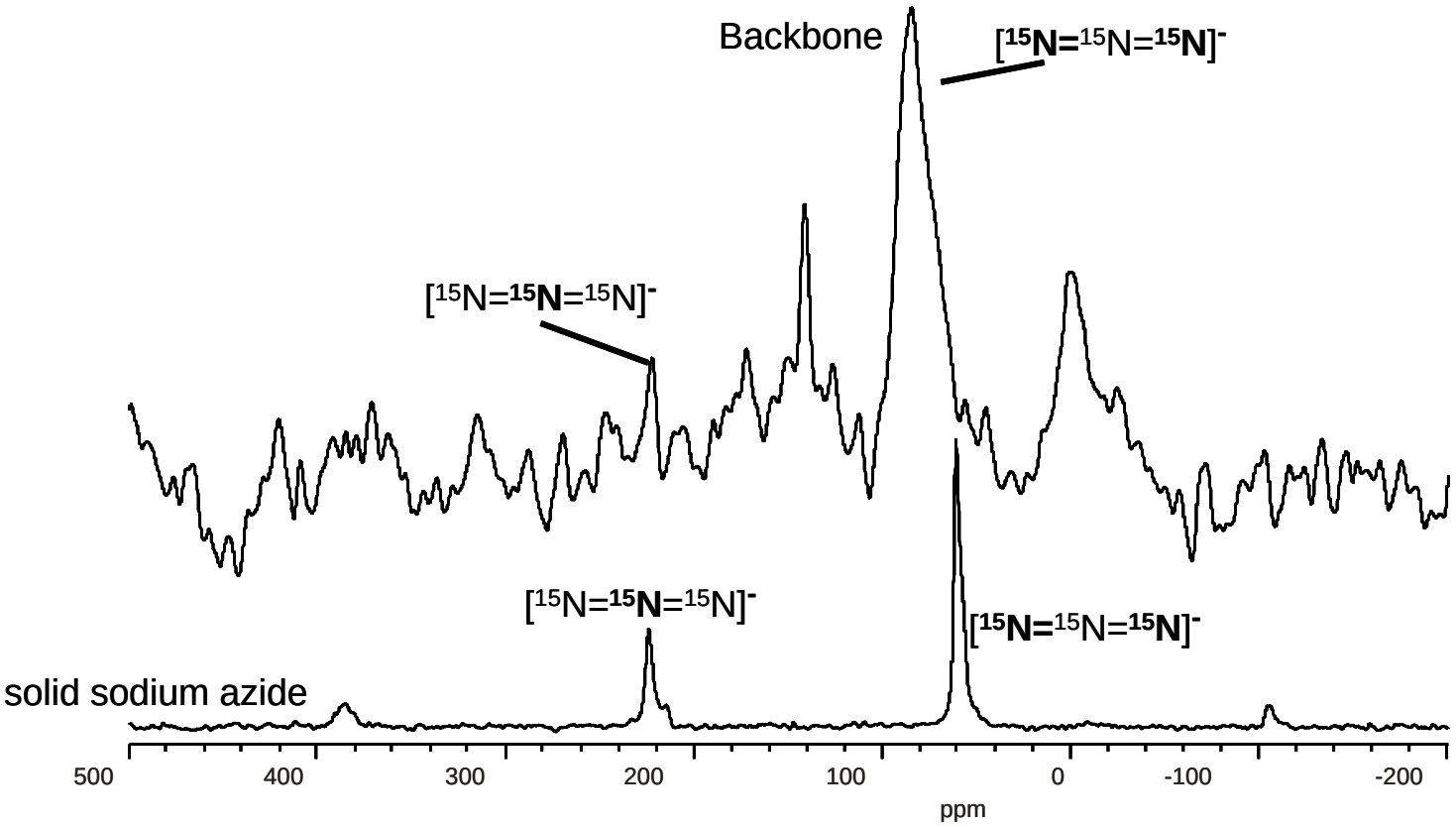
Backbone
[15N=15N=15N]-
[15N=15N=15N]-
[15N=15N=15N]-
solid sodium azide
500
400
300
200
100
0
-100
-200
ppm

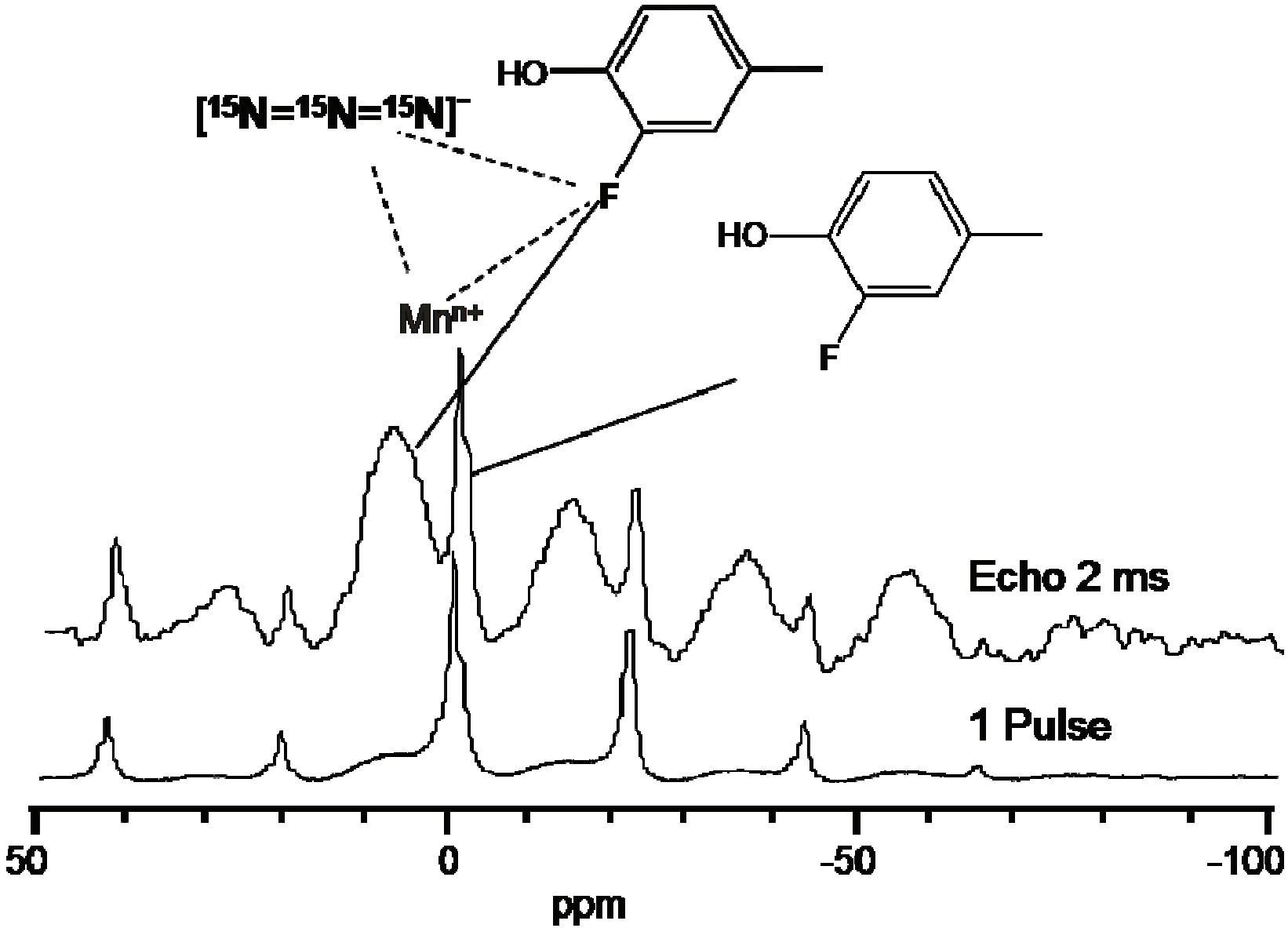
HO
[15N=15N=15N]−
F
HO
F
Mn n+
Echo 2 ms
1 Pulse
50
0
-50
-100
ppm

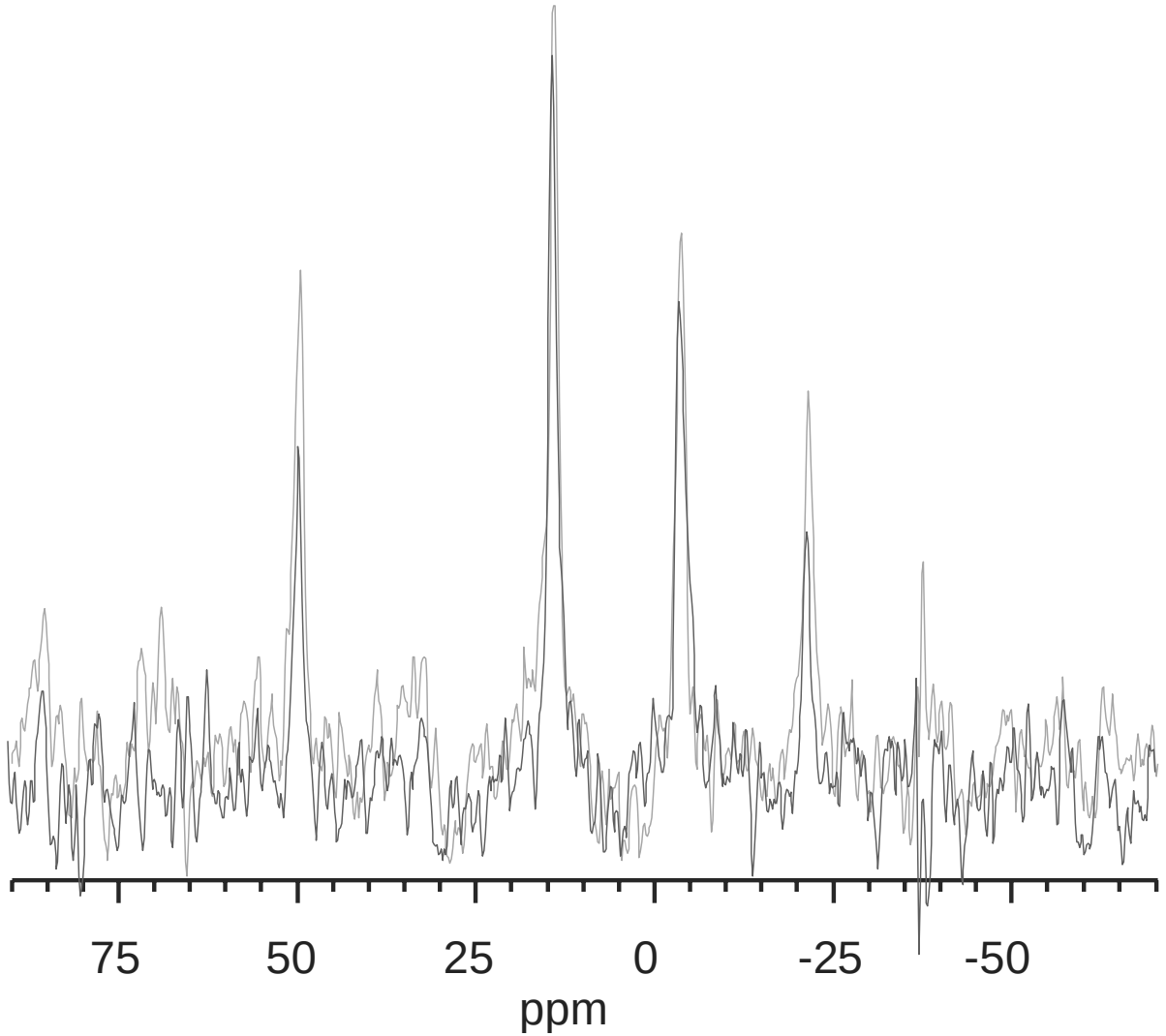
75
50
25
0
-25
-50
ppm

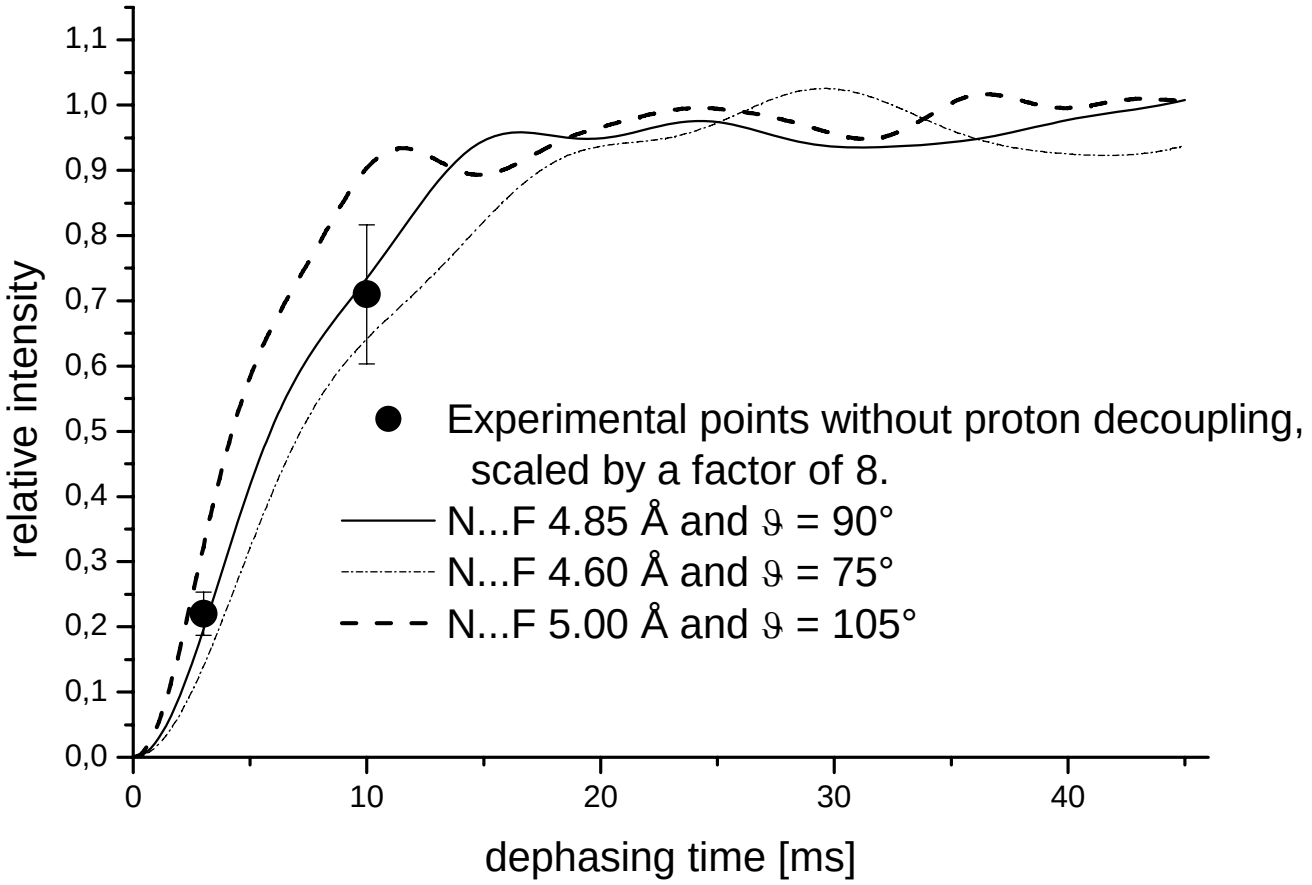
1,1
1,0
0,9
0,8
0,7
0,6
0,5
0,4
0,3
0,2
0,1
0,0
relative intensity
0
10
20
30
40
dephasing time [ms]
Experimental points without proton decoupling,
scaled by a factor of 8.
N...F 4.85 Å and ϑ = 90°
N...F 4.60 Å and ϑ = 75°
N...F 5.00 Å and ϑ = 105°

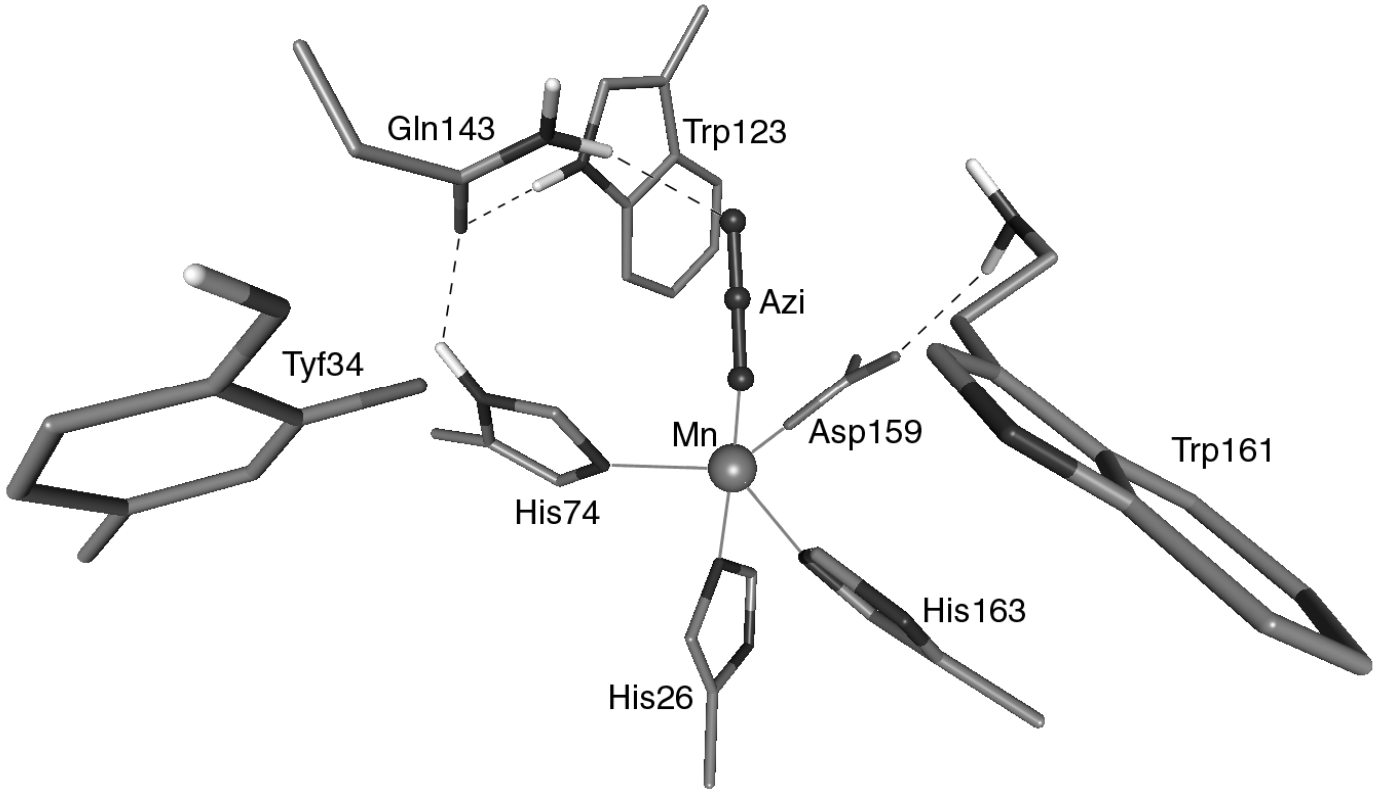
Gln143
Trp123
Azi
Tyf34
Mn
Asp159
Trp161
His74
His163
His26